Earth, Planets and Space

EXPRESS LETTER

Open Access

Crustal structure beneath earthquake swarm in the Noto peninsula, Japan

Junichi Nakajima*

Abstract

We carried out seismic tomography study to reveal three-dimensional (3D) seismic velocity structures in the Noto peninsula, Japan, where swarm-like seismic activity started in December 2020. The obtained results reveal a highly heterogeneous structure in the crust. The most striking feature is the existence of a low-velocity anomaly in the lower crust beneath the Noto earthquake swarm. Although the data set used in this study cannot resolve the upper mantle structure, previous regional tomographic studies suggest that a low-velocity anomaly exists at depths of 50–150 km around the Noto peninsula that is probably interpreted as a fluid-rich region. We infer that fluids have been supplied from the uppermost mantle to the lower crust over a geological time scale and a large volume of fluids have accumulated below the seismogenic zone beneath the Noto peninsula. A further upward migration of fluids to the upper crust, which may have suddenly started in December 2020, probably triggers numerous earthquakes at depths of 10–15 km. Since major active faults exist at shallower extensions of the hypocenters of the Noto earthquake swarm, we consider that the earthquake swarm occurs along pre-existing and weak fault planes. Dense temporary seismic observations will highlight a smaller-scale (5–10 km) 3D seismic velocity model and finer hypocenter distribution, which provide additional information for better understanding of the generation mechanisms of the Noto earthquake swarm.

Keywords: Travel-time tomography, Lower crust, Fluids, Aseismic slip

*Correspondence: nakajima@geo.titech.ac.jp

Department of Earth and Planetary Science, School of Science, Tokyo Institute of Technology, Meguro-ku, Japan

Graphical Abstract

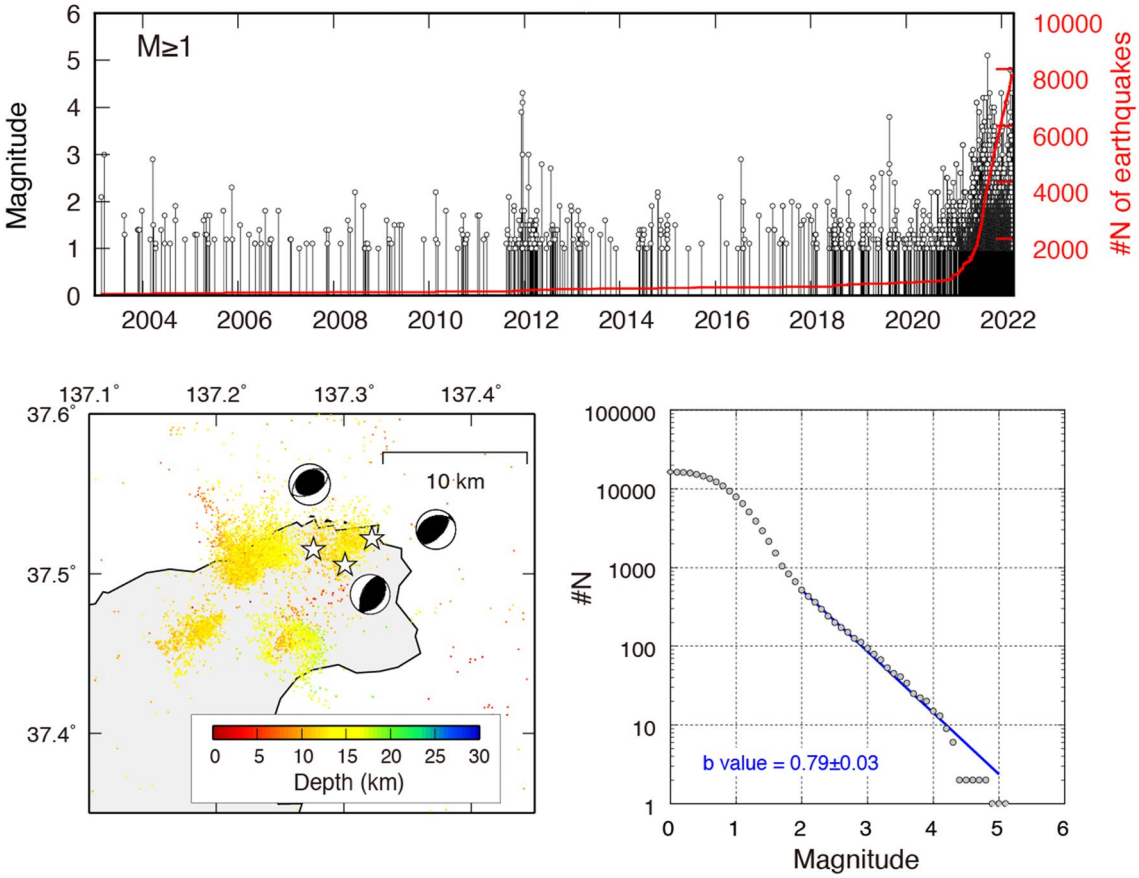

Introduction

The Noto peninsula is located in the Japan Sea side of central Japan, where no volcanisms occur since late Miocene. The largest earthquake beneath the Noto peninsula in the last 100 years was the M6.9 Noto-Hanto earthquake that occurred on March 25, 2007, at the northwestern part of the peninsula (Fig. 1a). Many aftershocks followed the mainshock, but aftershock activity was limited to the western part of the peninsula (Sakai et al. 2008). In December 2020, swarm-like seismic activity (Noto earthquake swarm) started at the northeastern tip of the Noto peninsula, and ~ 8000 earthquakes ($M \geq 1$) occurred as of March 2022 (Fig. 1b). The Noto earthquake swarm occurs in four somewhat separated areas within the lateral extent of ~ 15 km by ~ 15 km, and the hypocenters are mainly distributed at depths of 10–15 km (Fig. 1c). The frequency–magnitude distribution of the earthquake swarm shows a bend at $M \sim 1.5$, and b value for $M \geq 2$ is calculated to be 0.78 ± 0.03 with the maximum likelihood estimation method (Utsu, 1974) (Fig. 1d). The magnitudes of the earthquake swarm are generally small ($M \leq 3$), but three $M \geq 5.0$ earthquakes occurred around the northeastern cluster and their focal mechanisms show reverse faulting with a compressional axis of NW–SE (Fig. 1c). The total seismic moment released since December 2020 until November 15, 2021, is comparable to an earthquake with M_w6.7 (Hiramatsu 2022).

Nishimura et al. (2022) revealed that transient inflation with horizontal displacement of up to 12 mm and uplift of 30 mm is observed at permanent geodetic stations within 30 km from the epicentral region of the earthquake swarm. Assuming a spherical inflation (Mogi) source, the observed displacements can be explained by a volumetric increase of $\sim 2.5 \times 10^7$ m^3 at a depth of ~ 12 km. Nishimura et al. (2022) speculated that the volumetric increase is caused by upwelling fluids originally dehydrated from the subducted Pacific plate.

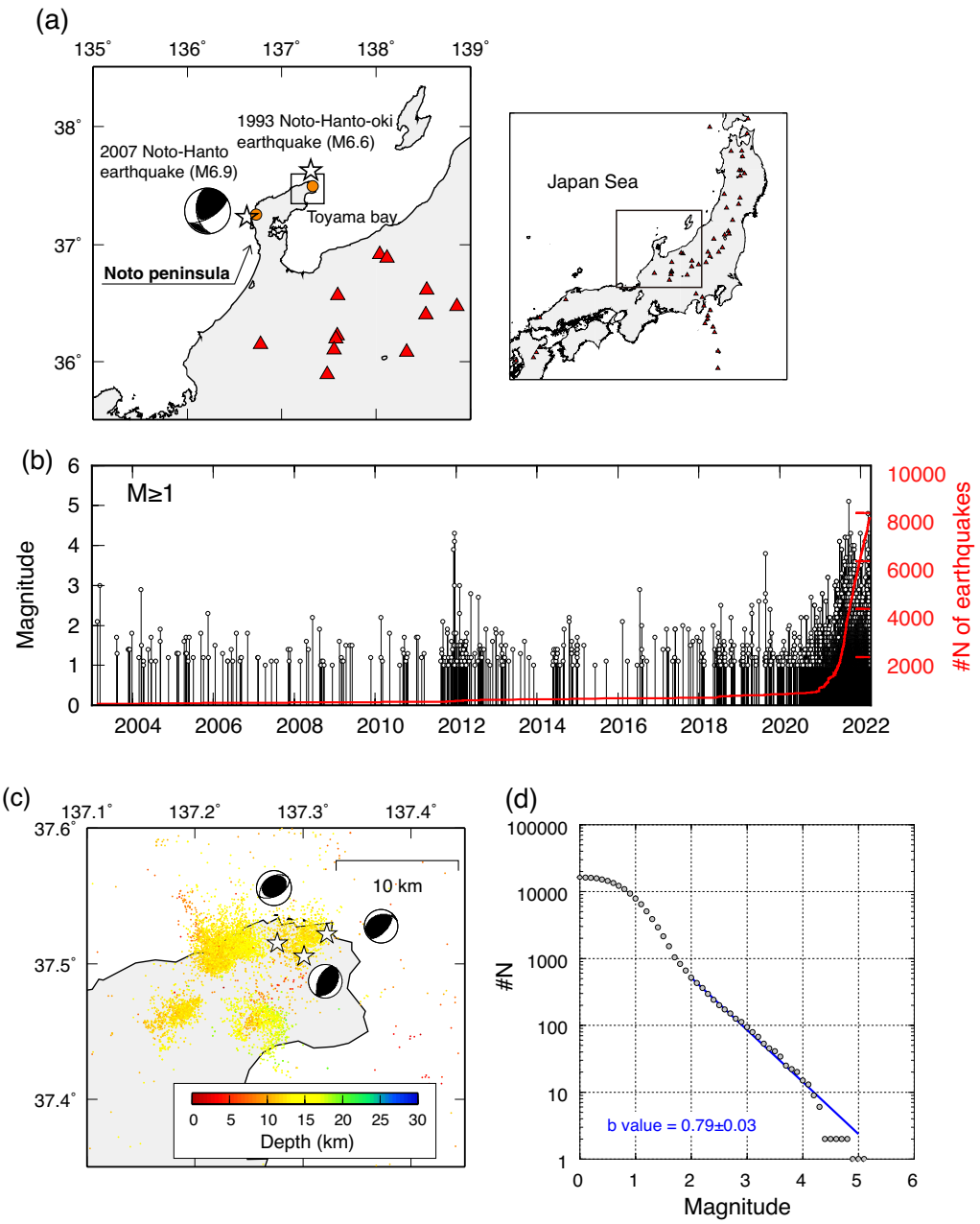

Fig. 1 **a** Map showing the study area. While stars denote the epicenters of the 1993 Noto-Hanto-oki and 2007 Noto-Hanto earthquakes. The F-net focal mechanism solution is shown for the 2007 event. Orange circles represent locations of two sites with $^{3}He/^{4}He$ ratios of > 2.0Ra (Umeda et al., 2009), and red triangles denote active volcanoes. The location of the area is shown in the inset map by a rectangle. **b** Magnitude–time plots (black) and cumulative number (red) of the Noto earthquake swarm ($M \geq 1$) shown in **c**. **c** An enlarged map of the Noto earthquake swarm. Colored dots denote earthquakes ($M \geq 1$) that occurred from January 2003 to March 2022. Epicenters of three $M \geq 5$ earthquakes (M5.1 on September 16, 2021, M5.4 on June 19, 2022, and M5.2 on June 20, 2022) are shown by white stars with the F-net focal mechanism solutions. **d** A frequency–magnitude distribution for earthquakes shown in **c**

However, the detailed crustal structure beneath the Noto earthquake swarm remains poorly understood.

This paper reports a preliminary result of local seismic tomography beneath the Noto peninsula using arrival-time data of the Japan Metrological Agency (JMA) catalog, which are recorded at a permanent seismograph network. Our objective is to determine three-dimensional (3D) *P*- and *S*-wave velocity structures and

discuss a spatial relationship between a zone of low-velocity anomaly in the crust and the occurrence of the Noto earthquake swarm.

Data, methods, and resolution tests

We first selected earthquakes ($M \geq 1$) ($N = 78{,}828$) from the JMA catalog that occurred at depths of 0–60 km in a period from January 2003 to December 2020. We then kept earthquakes that satisfied the condition $H_{dep} > D_{min}$, where H_{dep} is the depth of the earthquake and D_{min} is the epicentral distance to the nearest station with a *P*-wave arrival pick. This criterion enabled us to keep earthquakes whose focal depth was reasonably constrained by arrival-time data at the nearest station. In this manner, we obtained 37,268 earthquakes (Fig. 2a). Comparisons of hypocenters before and after applying the H_{dep}–D_{min} criterion are shown in Additional file 1: Figure S1. We used phase-picking data reported in the JMA catalog, and the total number of phase data for 37,268 earthquakes was 651,321 for *P* waves and 651,293 for S waves, which were recorded at 226 stations located in the study area (squares in Fig. 2b). We confirmed that most stations located in the Noto peninsula possess 1500–6500 ray paths for both *P* and *S* waves (Fig. 2b).

We used the tomographic method of Zhao et al. (1992) to estimate 3D seismic velocity structure in the study area. The model space was covered with horizontal grid nodes at a spacing of 0.2 (blue crosses in Fig. 2b) and vertical grid nodes at depths of 0, 5, 10, 15, 25, 40, 60, and 80 km. A simplified 1-D velocity structure used in the JMA routine work (Ueno et al. 2002) was adopted as the initial *P*-wave velocity model with a constant Vp/Vs value of 1.73. The Conrad and Moho discontinues determined by Katsumata (2010) were introduced in the model space. We did not introduce smoothing constraints in the tomographic inversion. The root mean squares of the arrival-time residuals for the initial model, 0.25 s for *P*-wave and 0.41 s for *S*-wave, were reduced to 0.15 s and 0.22 s, respectively, after five iterations.

To evaluate the adequacy of the ray coverage and the reliability of the obtained images, we carried out two checkerboard resolution tests (CRT) with different parameterizations. We assigned positive and negative velocity perturbations of 10% to alternate grid nodes or to every two grid nodes, and calculated travel times for the two models, respectively, to generate synthetic arrival-time data. Random noises corresponding to the phase-picking errors (a standard deviation of 0.05 s for the *P*-wave and 0.10 s for the *S*-wave) were added to the synthetic data, and the synthetic arrival-time data thus generated were inverted for the same earthquake–station pairs and model parameterizations as in the real inversion. Additional file 1: Figure S2 shows the results of the two CRTs at depths of 5, 10, 15, and 25 km. The checkerboard patterns around the Noto peninsula are considerably recovered at depths of 5 and 10 km but are moderately smeared at deeper depths even for the CRT that was assigned the velocity perturbations to every two

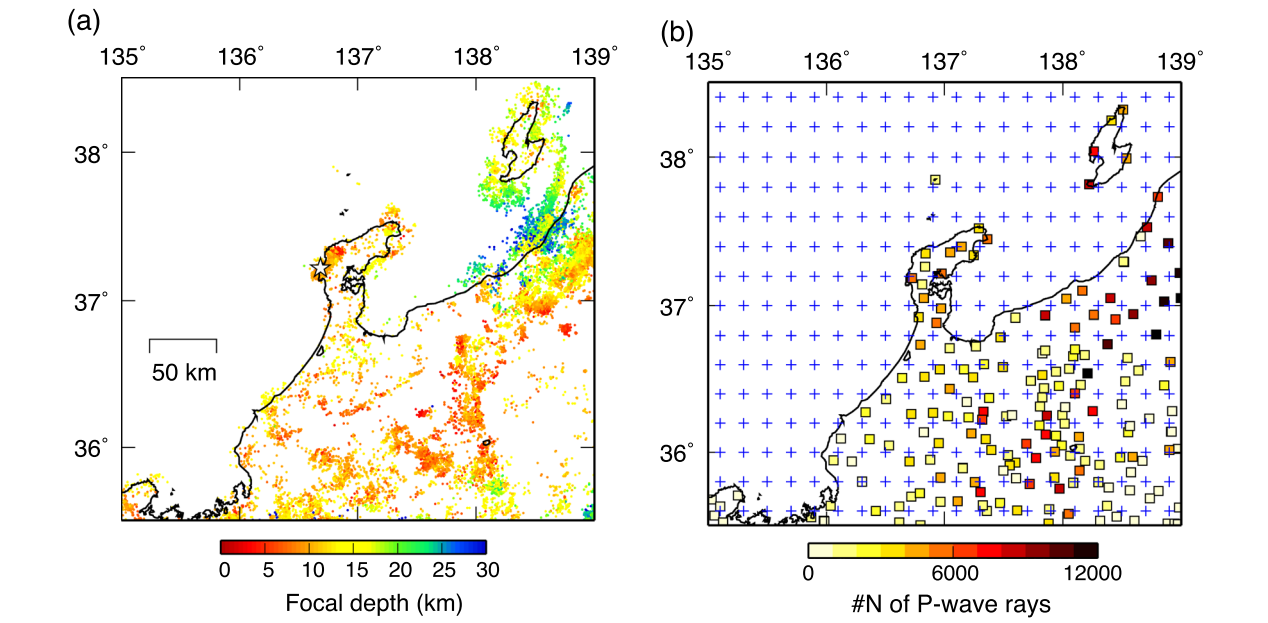

Fig. 2 **a** Distribution of earthquakes used in the tomographic inversion. Colors represent the focal depth. **b** The configuration of grid nodes (blue crosses) and the location of seismograph stations (squares). Colors of stations represent the number of *P*-wave ray paths recorded at each station

grid nodes (Additional file 1: Figure S2b). However, as discussed later, the results of other synthetic tests suggest the reliability of the large-scale (20–30 km) heterogeneities around the Noto peninsula. The spatial resolution of this study is higher than that of our previous studies (Nakajima and Hasegawa 2007a, b) because this study used more than tenfold number of crustal earthquakes and denser grid configurations to focus on the heterogeneous crustal structure beneath the Noto peninsula.

Results

The obtained 3D seismic velocity models show the existence of a highly heterogeneous structure beneath the Noto peninsula. Additional file 1: Figure S3 shows that a low-velocity anomaly is observed around the Noto peninsula at a depth of 5 km, and it exists around the hypocenter of the 2007 Noto-Hanto earthquake at depths of 10 and 15 km. The most striking observation is a distinct, NE–SW trending low-velocity anomaly distributed at a depth of 25 km from the epicenter of the 2007 Noto-Hanto earthquake to the Noto earthquake swarm.

The observed velocity anomalies are well represented along vertical cross sections. Figure 3 shows that the observed seismic velocities are high beneath the Toyama Bay at depths of > 10 km but are, relatively, low beneath the Noto peninsula. A distinct low-velocity anomaly is continuously distributed from the uppermost mantle to the upper crust beneath the source area of the 2007 Noto-Hanto earthquake (profiles A and B in Fig. 3). In contrast, a low-velocity feature appears to be limited in the lower crust in the central to the northeastern part of the peninsula (profiles C–G in Fig. 3). Value of Vp/Vs in the lower crust are overall high (≥ 1.8) beneath the 2007 Noto-Hanto earthquake and the earthquake swarm, but the high values beneath the earthquake swarm result from a combination of moderate Vp and low Vs (profiles F and G in Fig. 3). Figure 4 better characterizes the heterogeneities beneath the 2007 Noto-Hanto earthquake and the earthquake swarm. The low-Vs anomaly observed in the lower crust beneath the 2007 Noto-Hanto earthquake appears to be connected with that beneath the earthquake swarm (profiles H and I in Fig. 4), and the earthquake swarm occurs in a region below which there is a low-Vs anomaly beneath the seismogenic zone. We infer that the low-velocity anomaly in the lower crust is probably responsible for the occurrence of the Noto earthquake swarm. It is noted that we did not use earthquakes that occurred after January 2021 when the Noto earthquake swarm became much active and therefore the low-velocity anomaly beneath the swarm must have existed prior to its activation in December 2020.

We relocated > 91,000 earthquakes ($M \geq 1$) that occurred in the period from January 2003 to March 2022, using the 3D *P*- and *S*-wave velocity model obtained in this study. The relocated hypocenters became shallow by 1–2 km compared to the original JMA hypocenters beneath the earthquake swarm (Fig. 5a) as well as in a wider region of the study area (Additional file 1: Figure S4). The relocated hypocenters of the Noto earthquake swarm appear to be distributed along a SE-dipping plane, and major active faults exist at shallower extensions of the hypocenters (profiles M and O in Fig. 5). Since the SE-dipping plane is consistent with the strike and dip of one nodal plane of the focal mechanisms of $M \geq 5$ earthquakes (profile G in Fig. 3), the Noto earthquake swarm probably occurred along SE-dipping pre-existing fault planes.

To assess the reliability of the observed low-velocity anomaly in the lower crust beneath the Noto earthquake swarm, we carried out a sensitivity test focusing on that low-velocity anomaly. In the test, we assigned a NE–SW trending low-velocity anomaly at depths of ≥ 25 km beneath the Noto peninsula (model panels in Additional file 1: Figure S5). We calculated the synthetic arrival-time data for this model in the same manner as the CRT and conducted seismic tomography with the generated synthetic data set. The results demonstrated that the input velocity anomalies are well reproduced for both P and S waves in the northeastern part of the peninsula (profiles E–G in Additional file 1: Figure S5), even though the recovery of the input model is limited in the western part, in particular for S waves (profiles A–C in Additional file 1: Figure S5). We carried out another synthetic test, restoring resolution test (RRT) (Zhao et al. 1992), in which the 3D tomographic results obtained by inverting the real data were assumed as a synthetic model and synthetic data were generated for that 3D velocity model. When the restoring image obtained by inverting the synthetic data is similar to the real image, we consider that our data set can resolve the complicated velocity anomalies that are not introduced in CRTs. The results of RRT showed that the overall shape of the low-velocity anomaly in the lower crust beneath the Noto earthquake swam are reasonably well recovered for *P* waves but are slightly smeared for S waves (profiles E–G in Additional file 1: Figure S6).

Discussion

The presence of a fluid-rich zone has been suggested beneath the source area of the 2007 Noto-Hanto earthquake, based on travel-time tomography (e.g., Kato et al. 2008; Padhy et al. 2011), depth variation in the stress regime (Kato et al. 2011), and magnetotelluric survey (Yoshimura et al. 2008). The occurrence of the Noto-Hanto earthquake is discussed in the framework of the fluid-driven earthquakes or the fault-valve model (Sibson

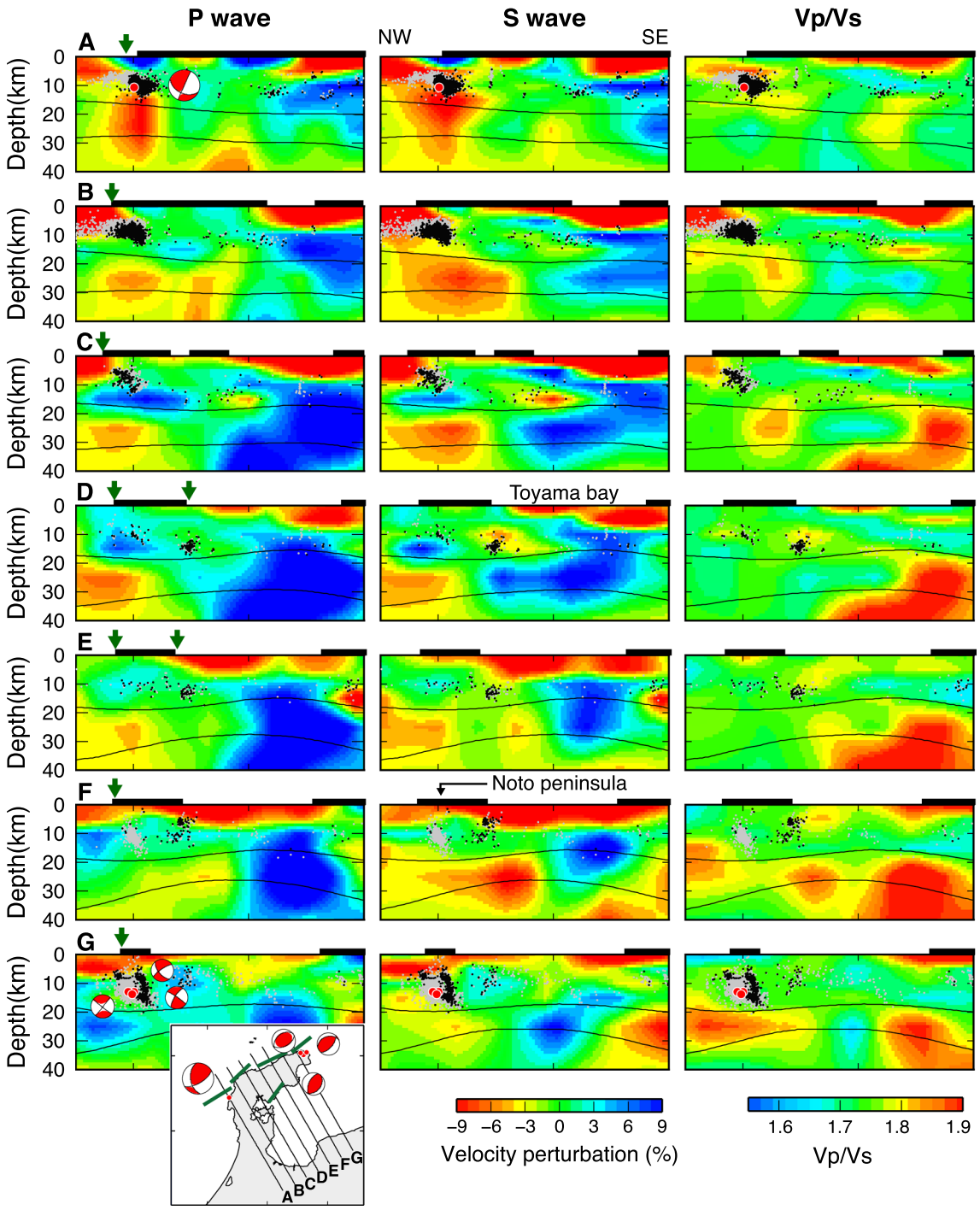

Fig. 3 Vertical cross sections of (left) *P*-wave and (middle) *S*-wave velocity perturbations, and (right) Vp/Vs ratios along seven profiles (**A**–**G**) shown in the inset map. Black and gray dots denote earthquakes within a 5-km-wide zone along each profile, which are used and are not used in the tomography inversions, respectively. Hypocenters of the earthquakes are relocated with the 3-D velocity model. The hypocenters and the F-net focal mechanisms for the 2007 M6.9 Noto-Hanto earthquake (profile **A**) and three $M \geq 5$ earthquakes in the Noto earthquake swarm (profile **G**) are shown by red circles and beachballs, respectively. The focal mechanisms are shown only on *P*-wave velocity images. Black curves denote the Conrad and Moho discontinuities (Katsumata, 2010) adopted in the inversion, and black bars on the surface represent the land areas. Green arrows on *P*-wave velocity images represent the surface location of the major active faults and segments (see the inset map). The direction of profiles and the locations of the Noto peninsula and Toyama bay are indicated on *S*-wave velocity images

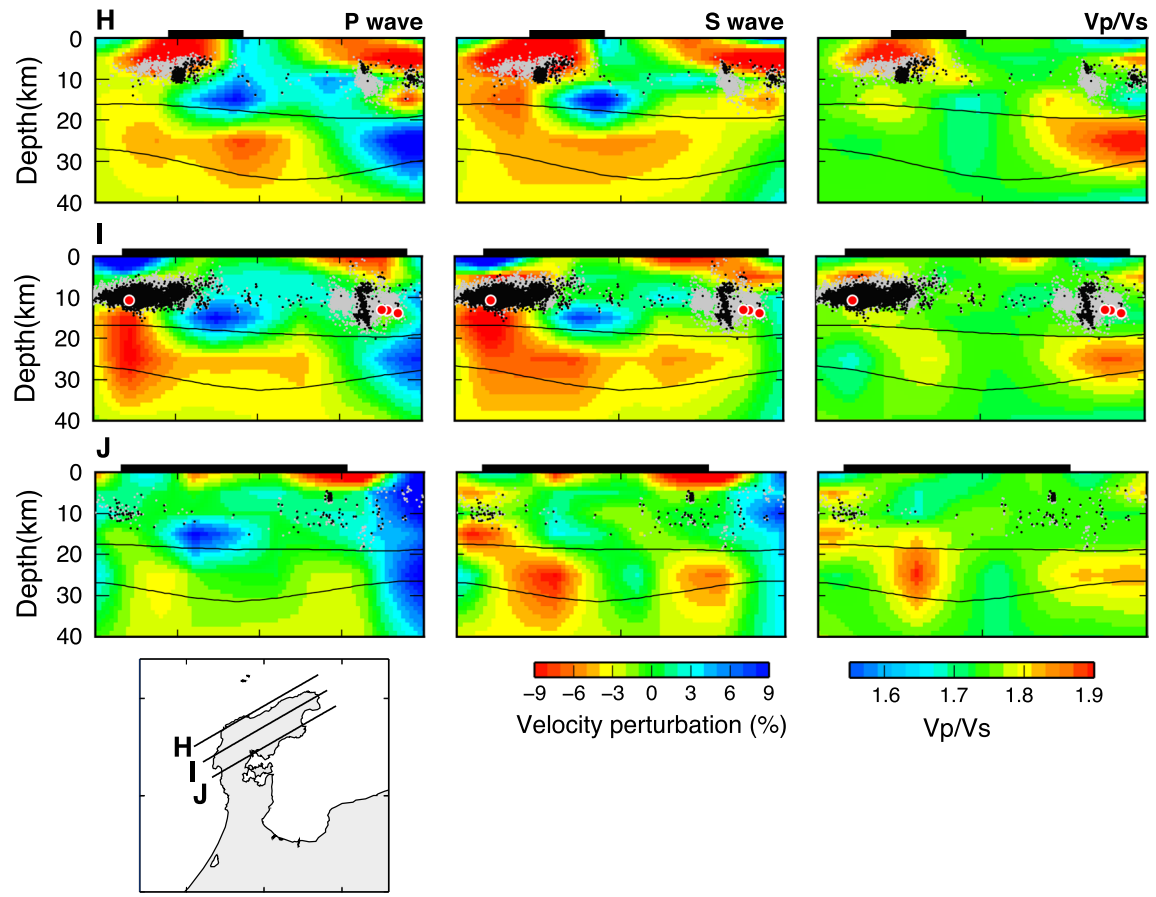

Fig. 4 Vertical cross sections of (left) *P*-wave and (middle) *S*-wave velocity perturbations, and (right) *Vp*/*Vs* ratios along three profiles (**H**–**J**) shown in the inset map. Other symbols are the same as in Fig. 3

2020), which can be supported by our observation that the low-velocity anomaly exists beneath the source area of the 2007 earthquake. This study further suggests that a fluid-rich zone in the lower crust extends continuously to the northeastern tip of the Noto peninsula, where an earthquake swarm was activated since December 2020.

Regional travel-time tomographic studies using teleseismic or local deep-focus earthquakes have shown that the uppermost mantle (depths of 50–150 km) beneath the Noto peninsula locally exhibits a low-velocity anomaly (Additional file 1: Figure S7) (e.g., Nakajima and Hasegawa 2007a; Zhao et al. 2012; Asamori and Zhao 2015). The low-velocity anomaly in the uppermost mantle appears to be separated from that beneath a volcanic area in central Japan where fluids derived from deep dehydration of both the Pacific and Philippine Sea slabs are probably supplied (e.g., Nakajima and Hasegawa 2007a; Nakamura et al. 2008). Although we have no conclusive argument for the origin of the low-velocity anomaly in the uppermost mantle beneath the Noto peninsula, we interpret that the low-velocity anomaly represents a fluid-rich area rather than high-temperature anomalies because no volcanisms occur in the Noto peninsula. Fluids may have been supplied from the uppermost mantle over a geological time scale and have accumulated in the lower crust beneath the Noto peninsula. The fluid abundant lower crust thus formed is probably imaged as the distinct low-velocity anomalies (Figs. 3, 4).

Umeda et al. (2009) showed that most hot springs in the Noto peninsula exhibit low $^{3}He/^{4}He$ ratios ranging from 0.03 to 1.2 Ra (Ra, the atmospheric $^{3}He/^{4}He$ ratio). However, $^{3}He/^{4}He$ ratios of two gas samples exceed 2.0 Ra (orange circles in Fig. 1a), and the two anomalous areas are located near the epicenters of the 1993 M6.6 Noto-Hanto-oki and 2007 Noto-Hanto earthquakes and the Noto earthquake swarm. Umeda et al. (2009) interpreted that the two areas with high $^{3}He/^{4}He$ ratios are probably attributable to the local upward migration of fluids with the mantle-derived helium and such fluids may have triggered the 1993 and 2007 earthquakes. These observations support our hypothesis that the mantle-derived fluids are supplied to the crust beneath the Noto peninsula.

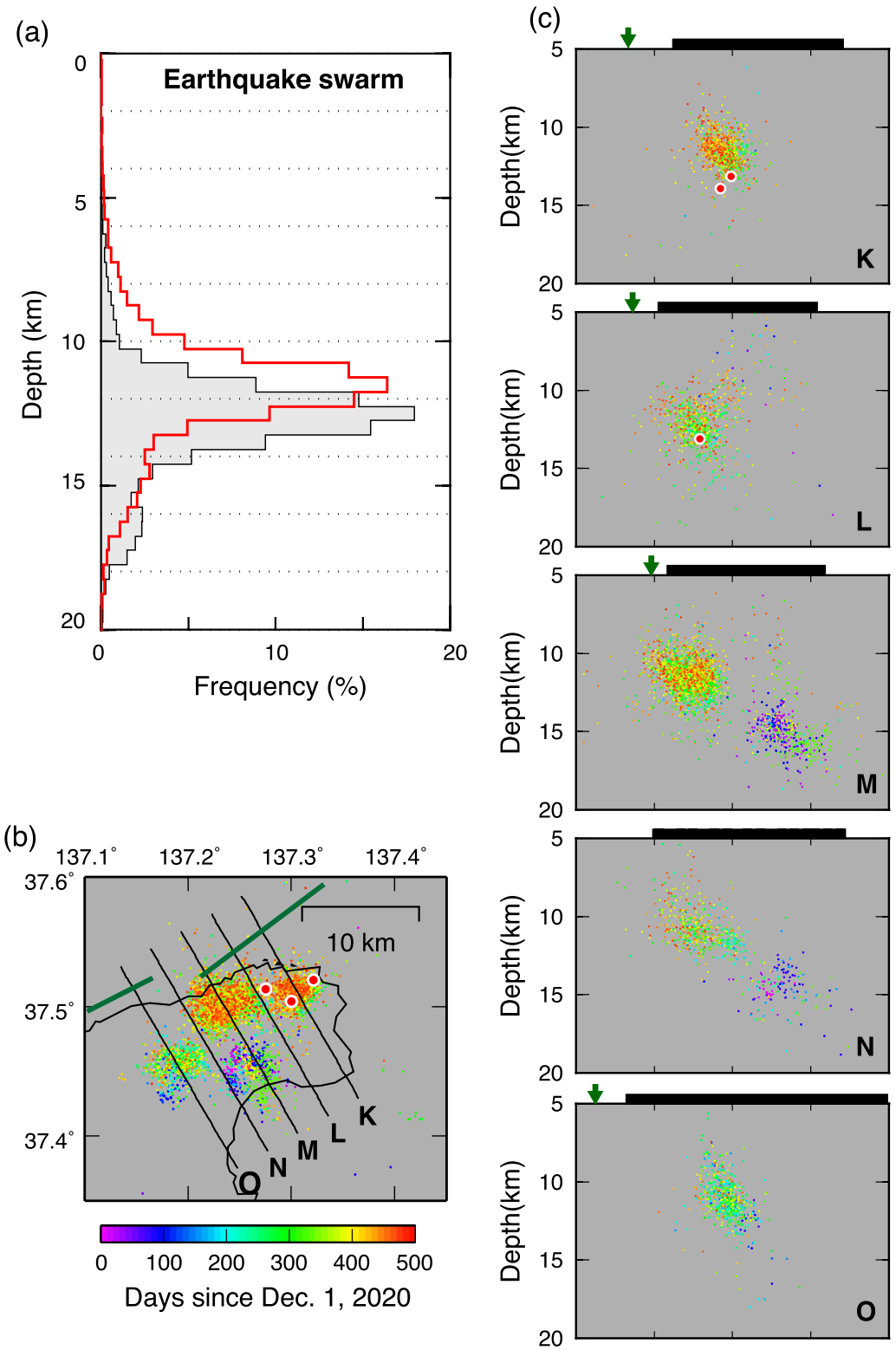

Fig. 5 **a** Histograms of focal depth of (gray) JMA original and (red) relocated hypocenters ($M \geq 1$) for the Noto earthquake swarm that occurred from January 2003 to March 2022 in an area shown in **b**. **b** The locations of relocated hypocenters ($M \geq 1$) with colors representing elapsed days from December 1st, 2020, when swarm activity started to be active. Green lines denote the location of the major active faults and segments. Red circles represent the epicenters of three $M \geq 5$ earthquakes. **c** Vertical cross section of relocated hypocenters along five profiles (K–O) shown in **b**. Colors represent elapsed days from December 1st, 2020. Other symbols are the same as in Fig. 3

We propose a three-step process to generate earthquake swarm beneath the Noto peninsula. A low-permeability seal beneath the seismogenic zone first breaks (Sibson 2020), which subsequently causes sudden upward migrations of a large volume of overpressurized fluids into individual faults in the upper crust. Since high pore-fluid pressures can stabilize shear slip at a rate-strengthening part of each fault by increasing the friction parameter (a–b) and reducing the critical stiffness (k_c) (e.g., Scholz 1998; Cappa et al. 2019; Bedford et al. 2021), aseismic slip could be triggered simultaneously along pre-existing faults. Moreover, high pore-fluid pressures weaken the shear strength of frictionally locked asperity patches on each fault. Therefore, a combined effect of enhanced aseismic slip and reduced strength of asperity patches probably induces incessant seismicity that is recognized as an earthquake swarm. The lateral extent of the earthquake swarm may be controlled by that of an area to which overpressurized fluids are intensively supplied. The earthquake swarm will cease when the rate of fluid supply to the upper crust becomes reduced.

Although the upward migration of mantle-derived fluids to the surface is suggested from the observations of $^3He/^4He$ ratios, the earthquake swarm is concentrated at depths of 10–15 km and few earthquakes occur at depths of $\leq$5 km (Figs. 3, 4, 5). A brittle behavior of rock is fundamentally required for the generation of earthquakes (e.g., Albaric et al. 2009), but the seismogenesis is limited in a depth range with negative a–b (e.g., Scholz 1998). Maeda et al. (2021) estimated the thickness of the seismogenic layer to be 4–6 km for pelitic and mafic rocks beneath another earthquake swarm (Wakayama swarm) in southwestern Japan. Even though the absolute depth of the seismogenic layer depends on the thermal structure, the inferred thickness is comparable to that of seismicity observed for the Noto earthquake swarm. The concentration of seismicity at depths of 10–15 km is probably controlled by the lithological and frictional properties of the crustal rocks.

A coupled process between the enhancement of aseismic slip and subsequent triggering of earthquakes has been observed for earthquake swarm along plate boundaries (e.g., Lohman and McGuire 2007) and in volcanic areas (e.g., Yukutake et al. 2022). Therefore, we infer that the coupled process is essential for triggering swarm activity. However, geodetic observations around the Noto peninsula suggest that surface deformation can be explained by an inflation of a spherical source, rather than by aseismic shear slip (Nishimura et al. 2022), and aseismic fault slip has not yet been geodetically detected. Detection of aseismic transients from earthquake data will provide additional and independent constraint on whether aseismic shear slip occurs (Llenos and McGuire 2011). Another issue that cannot be resolved in this study is upward migrations of the hypocenters, which are considered to occur as a response to the temporal and spatial migration of fluids or pore-fluid pressure diffusion (e.g., Malagnini et al. 2012; Yoshida and Hasegawa 2018). Figure 5(b), (c) suggests that swarm activity started at a depth of ~15 km and gradually expanded to a depth of ~10 km along the SE-dipping fault planes. However, the relocated hypocenters with the 3D velocity model do not have enough resolution to discuss the detailed temporal and spatial evolution of seismicity. Furthermore, this study has no observations to suggest what broke the low-permeability seal, even though the candidates would probably include either episodic aseismic deformation (Nakajima and Uchida 2018), or stress loading by external forces such as strong motion (Nakajima and Hasegawa 2021), or fast increases in pore-fluid pressure itself to some threshold value (Shapiro et al. 2018).

Conclusions

This study carried out tomographic study around the Noto peninsula using arrival-time data from 37,268 earthquakes recorded at 226 seismograph stations. The obtained results show that a low-velocity anomaly exists in the lower crust where the earthquake swarm was observed at depths of 10–15 km since December 2020. Although we cannot constrain the uppermost mantle structure beneath the Noto peninsula, regional tomographic studies suggest the existence of a large low-velocity anomaly at depths of 50–150 km. Therefore, we interpret that fluids are supplied to the lower crust beneath the Noto peninsula from the uppermost mantle. This idea is supported by high $He/^4He$ ratios observed near the epicenters of the 2007 Noto-Hanto earthquake and the Noto earthquake swarm. The permeation of a large volume of fluids into crustal faults may cause the occurrence of frequent aseismic slip, triggering numerous earthquakes recognized as an earthquake swarm.

This study reports a first and preliminary result of 3D seismic velocity structure beneath the Noto earthquake swarm using arrival-time data recorded at permanent seismograph stations. A dense temporal seismic network that covers the Noto peninsula is essential to estimate much finer-scale crustal structures and to resolve the spatial and temporal migration of swarm activity, while geodetic monitoring with dense temporary stations will improve the detectability of transient surface deformation and may shed light on hidden signals of aseismic fault slip. Dense seismic and geodetic observations can highlight physical and mechanical processes during the earthquake swarm, which will lead to better understanding of the generation mechanism of this non-volcanic earthquake swarm and activated fault structures.

Abbreviation
JMA: Japan Meteorological Agency.

Supplementary Information

The online version contains supplementary material available at https://doi.org/10.1186/s40623-022-01719-x.

Additional file 1: Figure S1. a Map showing distribution of the JMA hypocenters ($M \geq 1$) (gray dots) that occurred at depths of 0–60 km from January 2003 to March 2022. Colored dots denote earthquakes that satisfied the condition $H_{dep} > D_{min}$ (see text for details), which are used in the tomographic inversions. **b** Vertical cross sections of hypocenters along eight profiles **a**–**h** in **a** that occurred within 10 km from each profile. Black bars and red triangles on the surface represent the land areas and active volcanoes, respectively. **Figure S2.** Results of checkerboard resolution tests of *P* and *S* waves at depths of 5, 10, 15, and 25 km. **a** Results of velocity anomalies that assigned to alternate grid nodes. **b** Results of velocity anomalies that assigned to every two grid nodes. **Figure S3. a** *P*-wave and **b** *S*-wave velocity perturbations and **c** *Vp*/*Vs* ratios at depths of 5, 10, 15, and 25 km. Velocity perturbations are the deviations from the average velocity at each depth. Regions with the deviated weight sum of greater than 1000 are shown. Location of major active faults and segments are shown by green lines (see Hiramatsu, 2022). Distribution of hypocenters (gray dots) and the F-net focal mechanisms for the 2007 M6.9 Noto-Hanto earthquake and three $M \geq 5$ earthquakes in the Noto earthquake swarm are shown in the inset. **Figure S4.** Vertical cross sections of JMA original (black) and relocated (red) hypocenters ($M \geq 1$) with the 3D velocity model along seven profiles shown in the inset map. **Figure S5.** Results of sensitivity test of *P* and *S* waves **a** at a depth of 25 km and **b** along seven profiles. The model panels show the distribution of a velocity anomaly that assigned to the synthetic model (see text for details). **Figure S6.** Results of the real inversion and restoring resolution test of *P* (left) and *S* (right) waves along seven profiles shown in the inset map. **Figure S7.** Examples of regional tomographic study (modified from Nakajima and Hasegawa, 2007a). Distribution of *P*-wave velocity at a depth of **a** 40 and **b** 60 km. **c** A vertical cross section of *P*-wave velocity structure along profile A in **a**. The location of the Noto peninsula is indicated by an arrow. **d** The average *P*-wave velocities after the tomographic inversions derived from this study (red line) and from Nakajima and Hasegawa (2007a) (black line). *P*-wave velocity perturbations shown in each figure are the deviation from this average velocity. It is noted that this study cannot resolve seismic velocities at depths of ≥30 km (red dashed line).

Acknowledgements
We would like to thank D. Zhao for providing us with the tomography codes. Arrival-time data of earthquakes reported in the JMA-unified catalogue are used in this study. Discussion with A. Hasegawa was very fruitful, and fruitful comments by two anonymous reviewers improved the manuscript.

Author contributions
JN designed the research, analyzed the data, and wrote the manuscript. The author read and approved the final manuscript.

Funding
This work was supported by JSPS KAKENHI Grant Numbers JP20K20939 and JP21H01176 and by the Ministry of Education, Culture, Sports, Science, and Technology of Japan under its Observation and Research Program for the Prediction of Earthquakes and Volcanic Eruptions.

Availability of data and materials
We used arrival-time data of the JMA unified earthquake catalog and F-net focal mechanism solutions. These data are available from the web page of JMA (https://www.data.jma.go.jp/eqev/data/bulletin/index.html) and NIED (http://www.hinet.bosai.go.jp and https://www.fnet.bosai.go.jp/top.php?LANG=ja).

Declarations

Ethics approval and consent to participate
Not applicable.

Consent for publication
Not applicable.

Competing interests
The authors declare that they have no competing interests.

Received: 10 July 2022 Accepted: 12 October 2022
Published online: 01 November 2022

References

Albaric J, Déverchère J, Petit C et al (2009) Crustal rheology and depth distribution of earthquakes: insights from the central and southern east African rift system. Tectonophysics 468:28–41. https://doi.org/10.1016/j.tecto.2008.05.021

Asamori K, Zhao D (2015) Teleseismic shear wave tomography of the Japan subduction zone. Geophys J Int 203:1752–1772. https://doi.org/10.1093/gji/ggv334

Bedford JD, Faulkner DR, Allen MJ, Hirose T (2021) The stabilizing effect of high pore-fluid pressure along subduction megathrust faults: evidence from friction experiments on accretionary sediments from the Nankai Trough. Earth Planet Sci Lett 574:117161. https://doi.org/10.1016/j.epsl.2021.117161

Cappa F, Scuderi MM, Collettini C et al (2019) Stabilization of fault slip by fluid injection in the laboratory and in situ. Science Adv 5:1–9. https://doi.org/10.1126/sciadv.aau4065

Hiramatsu Y (2022) Seismic activities and seismotectonics in the northern Noto Peninsula. Rep CCCP 107:564–566 (**in Japanese**)

Kato A et al (2008) Three-dimensional velocity structure in the source region of the Noto Hanto earthquake in 2007 imaged by a dense seismic observation. Earth Planets Space 60:105–110. https://doi.org/10.1186/BF03352769

Kato A, Sakai S, Iidaka T et al (2011) Anomalous depth dependency of the stress field in the 2007 Noto Hanto, Japan, earthquake: potential involvement of a deep fluid reservoir. Geophys Res Lett 38:L06306. https://doi.org/10.1029/2010GL046413

Katsumata A (2010) Depth of the Moho discontinuity beneath the Japanese islands estimated by traveltime analysis. J Geophys Res 115:B04303. https://doi.org/10.1029/2008JB005864

Llenos AL, McGuire JJ (2011) Detecting aseismic strain transients from seismicity data. J Geophys Res 116:B06305. https://doi.org/10.1029/2010JB007537

Lohman RB, McGuire JJ (2007) Earthquake swarms driven by aseismic creep in the Salton Trough. California J Geophys Res 112:B04405. https://doi.org/10.1029/2006JB004596

Maeda S, Toda S, Matsuzawa T et al (2021) Influence of crustal lithology and the thermal state on microseismicity in the wakayama region, southern Honshu. Japan Earth Planets Space 73:173. https://doi.org/10.1186/s40623-021-01503-3

Malagnini L, Lucente FP, De Gori P et al (2012) Control of pore fluid pressure diffusion on fault failure mode: Insights from the 2009 L'Aquila seismic sequence. J Geophys Res 117:B05302. https://doi.org/10.1029/2011JB008911

Nakajima J, Hasegawa A (2007a) Subduction of the Philippine Sea plate beneath southwestern Japan: slab geometry and its relationship to arc magmatism. J Geophys Res 112:B08306. https://doi.org/10.1029/2006JB004770

Nakajima J, Hasegawa A (2007b) Deep crustal structure along the niigata-kobe tectonic Zone, Japan: Its origin and segmentation. Earth Planets Space 59:e5–e8. https://doi.org/10.1186/BF03352677

Nakajima J, Hasegawa A (2021) Prevalence of shallow low-frequency earthquakes in the continental crust. J Geophys Res Solid Earth 126:e2020JB021391. https://doi.org/10.1029/2020JB021391
Nakajima J, Uchida N (2018) Repeated drainage from megathrusts during episodic slow slip. Nature Geo 11:351–156. https://doi.org/10.1038/s41561-018-0090-z
Nakamura H, Iwamori H, Kimura J-I (2008) Geochemical evidence for enhanced fluid flux due to overlapping subducting plates. Nature Geo 1:630–630. https://doi.org/10.1038/ngeo290
Nishimura T, Nishikawa T, Sato D, Hiramatsu Y, Sawada A (2022) Ongoing crustal deformation and earthquake swarm in the Noto Peninsula, central Japan. EGU General Assembly 2022, Vienna, Austria, 23–27 May 2022, EGU22-10652. https://doi.org/10.5194/egusphere-egu22-10652
Padhy S, Mishra OP, Zhao D, Wei W (2011) Tectonophysics crustal heterogeneity in the 2007 Noto-Hanto earthquake area and its geodynamical implications. Tectonophys 509:55–68. https://doi.org/10.1016/j.tecto.2011.06.002
Sakai S, Kato A, Iidaka T et al (2008) Highly resolved distribution of aftershocks of the 2007 Noto Hanto earthquake by a dense seismic observation. Earth Planets Space 60:83–88. https://doi.org/10.1186/BF03352765
Scholz CH (1998) Earthquakes and friction laws. Nature 391:37–42. https://doi.org/10.1038/34097
Shapiro NM, Campillo M, Kaminski E et al (2018) Low-frequency earthquakes and pore pressure transients in subduction zones. Geophys Res Lett 45:11083–11094. https://doi.org/10.1029/2018GL079893
Sibson RH (2020) Preparation zones for large crustal earthquakes consequent on fault-valve action. Earth Planets Space 72:31. https://doi.org/10.1186/s40623-020-01153-x
Ueno H, Hatakeyama S, Aketagawa T, Funasaki J, Hamada N (2002) Improvement of hypocenter determination procedures in the Japan meteorological agency. Quart J Seism 65:123–134 (**in Japanese with English abstract**)
Umeda K, Ninomiya A, Negi T (2009) Heat source for an amagmatic hydrothermal system, Noto Peninsula. Central Japan J Geophys Res 114:B01202. https://doi.org/10.1029/2008JB005812
Utsu T (1974) A three-parameter formula for magnitude distribution of earthquakes. J Phys Earth 22:71–85. https://doi.org/10.4294/jpe1952.22.71
Yoshida K, Hasegawa A (2018) Hypocenter migration and seismicity pattern change in the yamagata-fukushima border, NE Japan, caused by fluid movement and pore pressure variation. J Geophys Res Solid Earth 123:5000–5017. https://doi.org/10.1029/2018JB015468
Yoshimura R, Oshiman N, Uyeshima M et al (2008) Magnetotelluric observations around the focal region of the 2007 Noto Hanto Earthquake (Mj 6.9). Central Japan Earth Planets Space 60:117–122. https://doi.org/10.1186/BF03352771
Yukutake Y, Yoshida K, Honda R (2022) Interaction between aseismic slip and fluid invasion in earthquake swarms revealed by dense geodetic and seismic observations. J Geophys Res Solid Earth 127:e2021JB022933. https://doi.org/10.1029/2021jb022933
Zhao D, Hasegawa A, Horiuchi S (1992) Tomographic imaging of P and S wave velocity structure beneath northeastern Japan. J Geophys Res 97:19909–19928. https://doi.org/10.1029/92jb00603
Zhao D, Yanada T, Hasegawa A et al (2012) Imaging the subducting slabs and mantle upwelling under the Japan Islands. Geophys J Int 190:816–828. https://doi.org/10.1111/j.1365-246X.2012.05550.x

Publisher's Note